Available online at www.sciencedirect.com
SCIENCE DIRECT®
Journal of Crystal Growth 266 (2004) 271–277
JOURNAL OF CRYSTAL GROWTH
www.elsevier.com/locate/jcrysgro

# Effects of baffle design on fluid flow and heat transfer in ammonothermal growth of nitrides

Q.-S. Chen[a,b], S. Pendurti[b], V. Prasad[b,*]

[a] *Institute of Mechanics, Chinese Academy of Sciences, 15 Bei Si Huan Xi Road, Beijing 100080, China*
[b] *Department of Mechanical and Materials Engineering, Florida International University, EC-2460, 10555 W Flagler St., Miami, FL 33174, USA*

**Abstract**

Efforts have been made in growing bulk single crystals of GaN from supercritical fluids using the ammonothermal method, which utilizes ammonia as fluid rather than water as in the hydrothermal process. Different mineralizers such as amide or azide and temperatures in the range of 200–600°C have been used to increase the solubility. The pressure is from 1 to 4 kbar. Modeling of the ammonothermal growth process has been used to identify factors which may affect the temperature distribution, fluid flow and nutrient transport. The GaN charge is considered as a porous media bed and the flow in the charge is simulated using the Darcy–Brinkman–Forchheimer model. The resulting governing equations are solved using the finite volume method. The effects of baffle design and opening on flow pattern and temperature distribution in an autoclave are analyzed. Two cases are considered with baffle openings of 15% and 20% in cross-sectional area, respectively.


*PACS:* 81.05.Ea; 81.10.Aj; 81.10.Dn

*Keywords:* A1. Computer simulation; A1. Fluid flows; A2. Hydrothermal crystal growth; A2. Top seeded solution growth; B1. Nitrides

## 1. Introduction

GaN and related materials can be used to fabricate blue/green/UV LEDs and LDs, and high temperature, high power electronic devices [1]. The LEDs can be used in cell phones and in the lighting and display equipments. LEDs can directly convert injected current into light and are very effective and longevous. GaN-based LEDs cover the expanded wavelength ranges from UV to IR. The nitrides also enable us to fabricate UV lasers, photodetectors, and high-power and high-speed transistors. For manufacture of LEDs and LDs, AlN or GaN substrates are lattice matched and isomorphic to nitride-based films. LEDs fabricated on sapphire substrates have a high dislocation density originating from a large lattice mismatch between GaN and sapphire substrates [2], and SiC substrates are expensive.

In past years, significant progress has been made to increase the size of nitride crystals. Porowski [3] used the ultra high-pressure method to grow GaN

*Corresponding author. Tel.: +1-305-348-2522; fax: +1-305-348-1401.
*E-mail address:* prasadv@fiu.edu (V. Prasad).

0022-0248/$ - see front matter © 2004 Published by Elsevier B.V.
doi:10.1016/j.jcrysgro.2004.02.055

single crystals from liquid Ga and $N_2$. Nitrogen pressures are in the range of 12–20 kbar and temperatures are from 1400°C to 1700°C. The nitrogen solubility in liquid gallium is in the order of 1% at 20 kbar. GaN plate-like single crystals of 100 $mm^2$ size and good crystallographic quality have been obtained. Mg-doped crystals were obtained by introduction of Mg into the growth solution.

Ketchum and Kolis [4] grew ammonothermal single crystals of gallium nitride in supercritical ammonia at 400°C and 2.4 kbar by using potassium amide ($KNH_2$) and potassium iodide (KI) as mineralizers. Hexagonal GaN crystal of $0.5 \times 0.2 \times 0.1\,mm^3$ was obtained. They recently used potassium azide ($KN_3$) or sodium azide ($NaN_3$) to increase the solubility of GaN in ammonia.

Aoki et al. [5] grew GaN single crystals with a maximum area of $3 \times 1.5\,mm^2$ and thickness of 1.0 mm from seeds at 850°C and 2 MPa of $N_2$ for 200 h by using the Na flux method. The maximum growth rate in the $c$ direction, about 4 μm/h at 850°C and 2 MPa of $N_2$, was higher than those in other directions and increased with growth temperature and $N_2$ pressure. This group recently grew single crystals of 10 mm size by using the molten sodium under 30–50 atm of nitrogen gas and 200–400°C. In these processes, sodium azide ($NaN_3$) and metal gallium were used. The key to the success was to use the high purity metallic sodium (more than 99.95%) and high purity pyrolytic BN crucible instead of sintered BN. This enabled the suppression of the growth of fine crystals at the boundary between the gas and the liquid, leading to the large size crystals.

Purdy et al. [6] grew both bulk cubic (zinc blende) and hexagonal GaN by ammonothermal reactions of gallium metal or $GaI_3$ under acidic ($NH_4Cl$, $NH_4Br$, or $NH_4I$) conditions. Gallium metal or compounds reacted slowly with supercritical $NH_3$ in the presence of acidic mineralizer forming GaN of 0.1 mm size as the only crystalline product at temperatures from 250°C to 500°C and pressure of 10,000 psi. Dwilinski et al. [7] obtained microcrystals of BN, AlN and GaN by the ammonothermal method using lithium or potassium amide as mineralizer at pressures in the range of 1–5 kbar and temperatures up to 550°C.

Ammonothermal growth processes have been modeled here using fluid dynamics, thermodynamics and heat transfer models. The particle charge is considered as a porous media bed and the flow in the porous charge is simulated using the Darcy–Brinkman–Forchheimer model.

## 2. Mathematical model

In the ammonothermal growth, predetermined amount of ammonia, mineralizers and GaN particles are loaded in the bottom of an autoclave, while seeds are hanged on a silver ladder made from 1.0 mm diameter Ag wire above a baffle with certain opening (Fig. 1). The baffle is made from 0.28 mm-thickness Ag foil and used to divide the autoclave into two parts—upper and lower portions. The part of the autoclave below the baffle is applied with a high temperature, $T_H$, and the part of the autoclave above the baffle, is applied with a low temperature, $T_L$. Two strap heaters are used on the sidewall of autoclave to obtain the required temperatures. A temperature gradient is achieved on the sidewall of the autoclave, e.g., 300–250°C

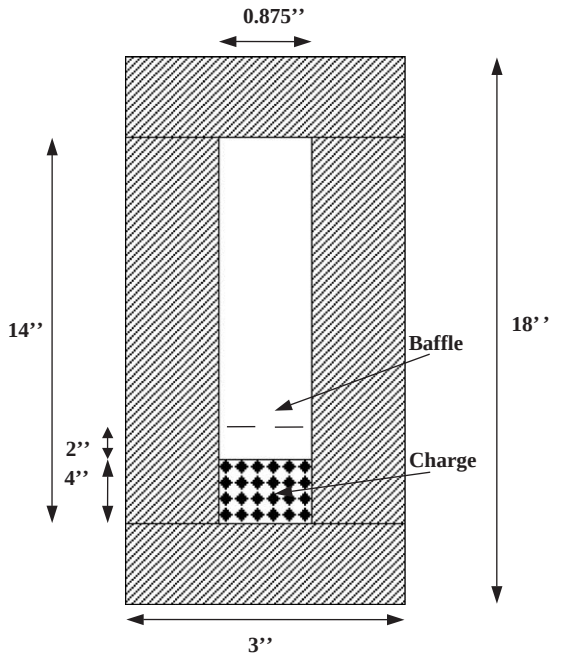


Fig. 1. Schematic of an ammonothermal growth system.

from the bottom to the top of the sidewall. In this paper, we consider a case in which the autoclave has an internal diameter of 0.875 inch (2.22 cm), external diameter of 3 inch, internal height of 14 inch (35.56 cm) and external height of 18 inch (Tem-Press MRA 378R with a volume of 134 ml). The charge height is 4 inch (10 cm), and the charge particle size is 0.6 mm. The baffle is located at a distance of 6 inch from the bottom of the autoclave. The maximum temperature difference applied on the sidewall of the autoclave, $\Delta T$, is 50 K.

A pressure of 2–4 kbar can be obtained with a 70–90% $NH_3$ fill. The pressure inside the autoclave can be estimated from the fill of ammonia from the equation of state (Predictive-Soave–Redlich–Kwong) [8]:

$$P = \frac{R_g T}{v-b} - \frac{a}{v(v+b)}, \tag{1}$$

where $v$ is the specific volume ($m^3$/mol), $R_g$ is the universal gas constant, $a = 0.42748 f(T_r) R_g^2 T_c^2 / P_c$, $b = 0.08664 R_g T_c / P_c$, and the reduced temperature $T_r = T/T_c$. For $T_r > 1$, $f(T_r) = [1 + c_1(1 - \sqrt{T_r})]^2$, where $c_1 = 0.9618$. The critical properties of ammonia are $T_c = 405.5$ K, and $P_c = 112.8$ bar. The reduced pressure and reduced temperature under typical ammonothermal growth conditions, e.g. 2000 bar and 250°C, are $P_r = 2000/112.8 = 17.7$, $T_r = 523/405.5 = 1.3$. For $P_r = 10$, and $T_r = 1.3$, the viscosity and conductivity of ammonia are $\mu/\mu_1 = 4.3$, $k/k_1 = 5.0$, respectively, where $\mu_1$ and $k_1$ are the dynamic viscosity, and thermal conductivity at 250°C and atmospheric pressure [9].

After the ammonothermal system is pressurized, ammonia occupies most of the volume. Hence the upper portion can be considered as a fluid layer with the assumption of incompressible flow and the Boussinesq approximation [10,11]. The GaN particles in the bottom of the autoclave can be considered as a porous medium. In this case, the Darcy–Brinkman–Forchheimer model can be employed in the porous layer, while Navier–Stokes equations can be used in the fluid layer [10,11]. The non-dimensional parameters of the system are listed below:

$$Ar = H/(2R), \quad Gr = g\beta R^3 \Delta T/\nu^2,$$
$$Pr = \nu/\alpha, \quad Da = K/R^2, \quad Fs = b/R, \tag{2}$$

where $Ar$, $Gr$, $Pr$, $Da$, $Fs$ denote aspect ratio, Grashof number, Prandtl number, Darcy number, and Forchheimer number, respectively. $H$ is the internal height of the autoclave, $R$ is the internal radius of the autoclave, $g$ is the acceleration due to gravity, $\beta$ is the isobaric coefficient of expansion, $\nu$ is the kinematic viscosity, and $\alpha$ is the thermal diffusivity. The permeability of porous matrix $K = d_p^2 \varepsilon^3/[150(1-\varepsilon)^2]$, where $\varepsilon$ is the porosity and $d_p$ is the average diameter of the nutrient particles. The Forchheimer coefficient $b = 1.75K^{0.5}/(\sqrt{150}\varepsilon^{1.5})$.

The governing equations in the porous and fluid layers can be combined by defining a binary parameter $B$ as: $B = 0$ in the fluid layer and $B = 1$ in the porous layer, respectively. The porosity $\varepsilon = 0$ in solid, $0 < \varepsilon < 1$ in porous layer and $\varepsilon = 1$ in fluid layer, respectively. The combined governing equations in a cylindrical coordinate system are:

$$\frac{\partial(\varepsilon\rho_f)}{\partial t} + \nabla\cdot(\rho_f \mathbf{u}) = 0, \tag{3a}$$

$$\frac{\rho_f}{\varepsilon}\frac{\partial \mathbf{u}}{\partial t} + \frac{\rho_f}{\varepsilon}(\mathbf{u}\cdot\nabla)\frac{\mathbf{u}}{\varepsilon} = -\nabla p + \rho_f g\mathbf{z} + \nabla\cdot(\mu_e\nabla\mathbf{u}) - B\left[\left(\frac{\mu_f}{K} + \frac{\rho_f b}{K}|\mathbf{u}|\mathbf{u}\right)\right], \tag{3b}$$

$$(\rho c_p)_e \frac{\partial T}{\partial t} + (\rho c_p)_f[(\mathbf{u}\cdot\nabla)T] = \nabla\cdot(k_e\nabla T), \tag{3c}$$

where $\mathbf{u}$, $T$, $\rho$, $k$, $c_p$ denote the velocity vector, temperature, density, thermal conductivity, and isobaric specific heat, respectively, $|\mathbf{u}|$ denotes the length of the velocity vector, $\mathbf{z}$ is the unit vector in the $z$ direction. Subscripts f and e denote fluid and effective, respectively.

A temperature profile is set on the sidewall of the autoclave, $T = T_H$, $z < H_B - 0.5\delta_T$; $T = T_H - (T_H - T_L)/\delta_T(z - H_B + 0.5\delta_T)$, $H_B - 0.5\delta_T \leqslant z \leqslant H_B + 0.5\delta_T$; $T = T_L$, $z > H_B + 0.5\delta_T$, where $H_B$ is the height of the baffle, and $\delta_T$ is the distance between the two strap heaters with $T_H$ and $T_L$. The top and bottom of the autoclave are considered adiabatic. The temperature distribution is considered axisymmetric, $\partial T/\partial r = 0$, at $r = 0$.

The governing equations are non-dimensionalized, and the reference velocity and time scale are $u0 = \nu/R = 1.4 \times 10^{-5}$ m/s and $t0 = R^2/\nu = 748$ s

for the present studies. The resulting governing equations are solved using the finite volume method. For the temperature equation, a profiled temperature boundary conditions are applied on the outer surfaces of the autoclave. For solving the momentum equations and the pressure equation inside the autoclave, we search the fluid boundaries inside the autoclave in $r$ and $z$ directions, respectively. For example, when solving the equations using the TDMA method, we search the fluid boundaries in $r$ or $z$ direction separately, and solve the equations in this direction in different intervals of fluid space. This way, we can obtain the fluid field inside the autoclave that contains different shapes of baffles and seeds. Grid used here is $208 \times 72$, and time step is $dt/t0 = 2 \times 10^{-6}$.

## 3. Results and discussions

Baffle design is essential for the successful growth of GaN crystals. Baffle is used to separate the growth zone from the dissolving zone, and to maintain a temperature difference between the two zones. For solubility curve with a positive coefficient of temperature, the growth zone is maintained at a lower temperature than that in the dissolving zone, thus the nutrient becomes supersaturated in the growth zone.

Fig. 2 shows some solubility data of GaN for mineralizers of $KN_3$, $KNH_2$/KI. It can be seen from Fig. 2 that the solubility of GaN for

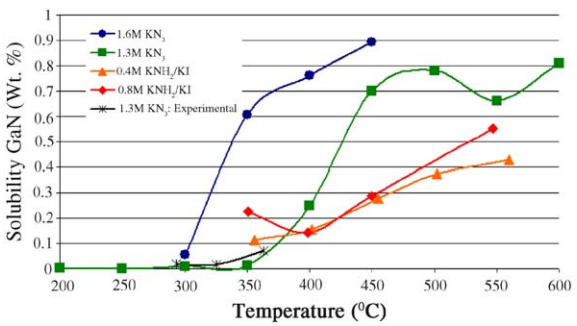


Fig. 2. Some solubility data of GaN from solubility experiments except symbol * representing data from seeded growth experiment (courtesy of Prof. Kolis at Clemson University).

mineralizer of 1.6 M $KN_3$ is high in the temperature range of 300–450°C. It seems that by using azide as mineralizer, a high solubility of GaN can be obtained at low growth temperatures. For 0.8 M $KNH_2$/KI, the solubility is low in the range of 350–550°C. Mineralizer of 2–6 M $KNH_2$ or $NaNH_2$ were now used to increase the solubility of GaN. With a fill of 60–85% and temperature of 600°C, pressure is about 35 kpsi. A typical run takes 14–21 days and some of the growth was on walls of the autoclave.

For the present study, the aspect ratio, Grashof number, Prandtl number, Darcy number and Forchheimer number are, $Ar = 16$, $Gr = 6.0 \times 10^7$, $Pr = 0.73$, $Da = 3.8 \times 10^{-6}$, and $Fs = 1.1 \times 10^{-3}$, respectively. Fig. 3a shows the flow pattern for a system with a baffle opening of 15% in cross-sectional area, e.g., 10% in the central hole and 5% in the ring opening between the baffle and the sidewall of autoclave. The flow is very weak in the porous layer, and the flow in the fluid layer is much stronger. The modified Grashof number can be used to measure the flow strength in the porous charge, $Gr^* = Gr \cdot Da$. In this case, the modified Grashof number is $Gr^* = 228$. Thus, the heat and mass transfer in the porous layer is mainly by conduction and diffusion. This may constraint the transport of nutrient between the charge and the fluid layer, and cause deposition on the sidewall of the autoclave as observed in experiments.

The temperature distribution is shown in Fig. 3b. The charge has the temperature of $T_H$ as applied on the lower part of the autoclave. Large temperature gradient exists at the fluid/charge interface and the fluid/autoclave interface. Supersaturation in the fluid is related to the temperature difference between the charge and the fluid layer. Large temperature gradient at the fluid/charge interface may cause large supersaturation, and subsequently nucleation near the fluid/charge interface.

Fig. 4a shows the fluid flow in an autoclave with a baffle opening of 20% in cross-sectional area, e.g., 10% in the central hole and 10% in the ring opening between the baffle and the sidewall of autoclave. The flow pattern is similar to that in the previous case. The flow goes up in the ring opening

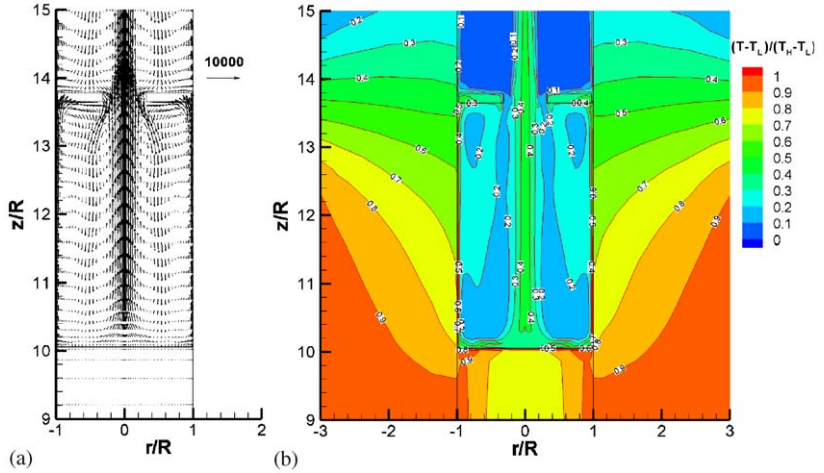


Fig. 3. (a) Fluid flow and (b) temperature field in a system with a baffle opening of 15% in cross-sectional area (central opening of 10% and ring opening of 5%).

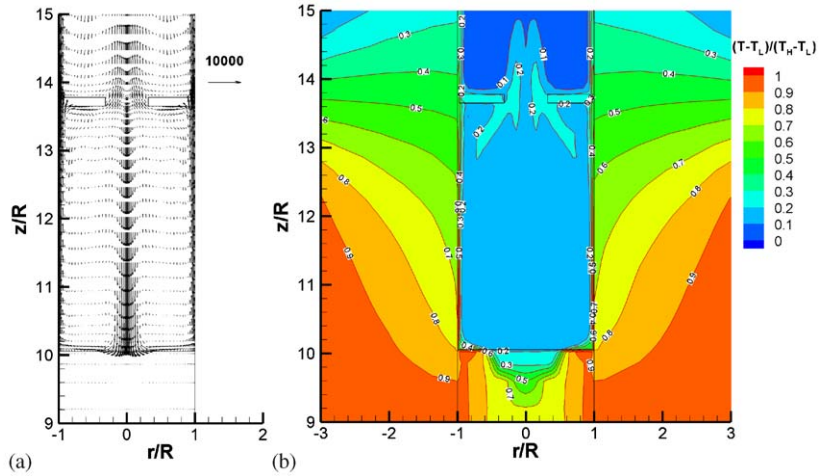


Fig. 4. (a) Fluid flow and (b) temperature field in a system with a baffle opening of 20% in cross-sectional area (central opening of 10% and ring opening of 10%).

between the baffle and the sidewall of the autoclave and comes back in the central opening causing strong mixing of fluid across the baffle. The temperature distribution is shown in Fig. 4b. The temperature difference across the baffle is smaller in Fig. 4b than that in Fig. 3b. The baffle opening is used to control the mixing of nutrients in the two zones, thus the transfer of nutrient from the lower part to the upper part. A larger baffle opening means more fluid mixing across the baffle and less temperature difference between the two zones.

The mixing of flow across the baffle can be seen from Fig. 5, which shows the changes of the vertical velocity at the center of the central hole opening in certain time period. The patterns of oscillations of velocity are repeatable for a longer time period than that shown in Fig. 5. The heating on the bottom and cooling on the top promote the Bénard-type convection in the fluid layer, which

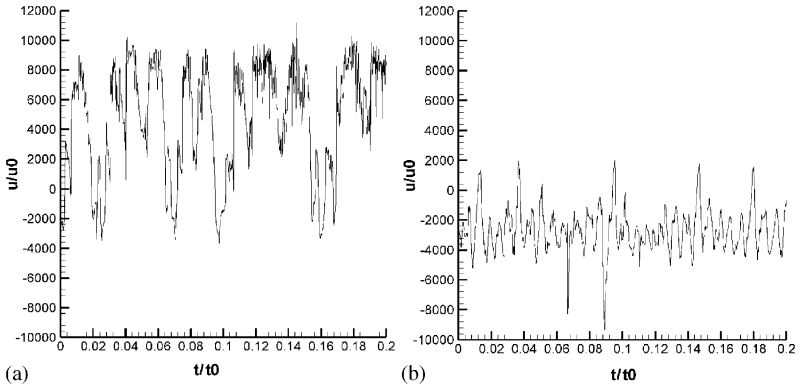


Fig. 5. Changes of the vertical velocity with time at the center of the central hole opening: (a) opening of 15%; and (b) opening of 20%.

interacts with the vertical temperature boundary layer near the sidewall of the autoclave, causing the unsteady and oscillatory flow. For a long time period, it is observed that the amplitude of velocity oscillation in the center of the central hole is larger for opening of 15% than that for opening of 20%. For opening of 15%, the vertical velocity in the center of the central hole changes directions over time. For opening of 20%, the vertical velocity in the center of the central hole is negative most of the time and the flow is mixed more thoroughly across the baffle, since the ring opening and the central opening are both 10% of the cross-sectional area. For opening of 20%, the amplitude of oscillation of velocity in the central opening is smaller than that in the case of 15% opening.

The constraints for the ammonothermal growth include dissolving of charge, nucleation on the sidewall, transfer of nutrient from charge to seed, and growth kinetics. The mass transfer between the charge and the fluid layer is important for the successful growth. The flow strength in the fluid layer depends on Grashof number, which is proportional to the temperature difference on the sidewall and the cubic of the internal radius of the autoclave. Flow in the charge layer depends on the modified Grashof number, product of Grashof number and Darcy number, which is proportional to the square of the average diameter of particles. The flow strength in the porous layer can be increased by increasing the size of particles, or by putting particles in bundles as in the hydrothermal growth. Effects of particle size on the flow pattern and temperature distribution in the autoclave can be found in Ref. [12]. Two-dimensional calculations are for case studies, and for three-dimensional calculations one can refer to Ref. [10].

## 4. Conclusions

An ammonothermal growth system is considered here in which the autoclave used has a volume of 134 ml, internal diameter of 0.875 inch (2.22 cm), and internal height of 14 inch (35.56 cm). Two cases are considered with baffle opening of 15% and 20% in cross-sectional area, respectively. The flow is weak in the charge and temperature gradient is large at the fluid/charge interface for both cases meaning large supersaturation and possible nucleation near the interface. In the case of opening of 20%, there is more fluid mixing across the baffle and less temperature difference between the two zones. The amplitude of oscillation of the vertical velocity in the center of the central hole in the case of 20% opening is smaller than that in the case of 15% opening since the ring opening and the central opening are both 10% of the cross-sectional area in the previous case. Baffle opening is carefully chosen to achieve certain temperature difference across the baffle, and thus the supersaturation above the baffle and growth rate of crystals. Other factors such as the particle size and charge height are also important parameters to be considered.

## Acknowledgements

Research is supported by DoD MURI program administered by the Office of Naval Research under Grant N00014-01-1-0716 and monitored by Dr. C.E. Wood. The authors would like to thank J.W. Kolis at Clemson University for providing the solubility data.

## References

[1] S.J. Pearton, R.J. Shul, F. Ren, MRS Internet J. Nitride Semicond. Res. 5 (2000) 11.
[2] S. Nakamura, M. Senoh, S. Nagahama, N. Iwasa, T. Matushita, T. Mukai, MRS Internet J. Nitride Semicond. Res. 4S1 (1999) G1.1.
[3] S. Porowski, MRS Internet J. Nitride Semicond. Res. 4S1 (1999) G1.3.
[4] D.R. Ketchum, J.W. Kolis, J. Crystal Growth 222 (2001) 431.
[5] M. Aoki, H. Yamane, M. Shimada, S. Sarayama, F.J. DiSalvo, Mater. Lett. 56 (2002) 660.
[6] A.P. Purdy, S. Case, N. Muratore, J. Crystal Growth 252 (2003) 136.
[7] R. Dwilinski, R. Doradzinski, J. Garczynski, L. Sierzputowski, M. Palczewska, A. Wysmolek, M. Kaminska, Internet J. Nitride Semicond. Res. 3 (1998) 25.
[8] K. Fischer, J. Gmehling, Fluid Phase Equilibria 112 (1995) 1.
[9] A.J. Chapman, Heat Transfer, Macmillan Publishing Company, New York, 1984.
[10] Q.-S. Chen, V. Prasad, A. Chatterjee, J. Larkin, J. Crystal Growth 198–199 (1999) 710.
[11] Q.-S. Chen, V. Prasad, A. Chatterjee, J. Heat Transfer 121 (1999) 1049.
[12] Q.-S. Chen, V. Prasad, W.R. Hu, J. Crystal Growth 258 (2003) 181.